

RESEARCH ARTICLE



Natural product sennoside B disrupts liquid-liquid phase separation of SARS-CoV-2 nucleocapsid protein by inhibiting its RNA-binding activity

Da-Wei Zhang^a, Xiao-Shuang Xu^a, Liangxu Xie^a, Lei Xu^a, Zhiguo Fu^b, Yimin Li^c and Xiaojun Xu^a 

^aInstitute of Bioinformatics and Medical Engineering, School of Electrical and Information Engineering, Jiangsu University of Technology, Changzhou, China; ^bDepartment of Orthopedics, Changzhou Hospital of Traditional Chinese Medicine, Changzhou, China; ^cCollege of Pharmacy and Key Laboratory for Research and Development of "Qin Medicine" of Shaanxi Administration of Chinese Medicine, Shaanxi University of Chinese Medicine, Xixian New District, China

ABSTRACT

The nucleocapsid protein (NP) of SARS-CoV-2, an RNA-binding protein, is capable of undergoing liquid-liquid phase separation (LLPS) during viral infection, which plays a crucial role in virus assembly, replication, and immune regulation. In this study, we developed a homogeneous time-resolved fluorescence (HTRF) method for identifying inhibitors of the SARS-CoV-2 NP-RNA interaction. Using this HTRF-based approach, we identified two natural products, sennoside A and sennoside B, as effective blockers of this interaction. Bio-layer interferometry assays confirmed that both sennosides directly bind to the NP, with binding sites located within the C-terminal domain. Additionally, fluorescence recovery after photobleaching (FRAP) experiments revealed that sennoside B significantly inhibited RNA-induced LLPS of the NP, while sennoside A displayed comparatively weaker activity. Thus, the developed HTRF-based assay is a valuable tool for identifying novel compounds that disrupt the RNA-binding activity and LLPS of the SARS-CoV-2 NP. Our findings may facilitate the development of antiviral drugs targeting SARS-CoV-2 NP.

ARTICLE HISTORY

Received 20 January 2025
Revised 2 April 2025
Accepted 29 April 2025

KEYWORDS

SARS-CoV-2; nucleocapsid protein; sennoside B; liquid-liquid phase separation; HTRF

Introduction



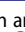

The severe acute respiratory syndrome coronavirus type 2 (SARS-CoV-2) has resulted in one of the deadliest pandemics in human history, known as coronavirus disease 2019 (COVID-19)¹. To date, approximately 770 million confirmed COVID-19 cases and over 7 million deaths have been reported globally, posing a significant threat to public health and economic development (World Health Organisation data, <https://data.who.int/dashboards/covid19/cases?n=0>, accessed on September 21, 2024). The novel coronavirus is highly transmissible and mutates rapidly, placing even vaccinated individuals at risk of infection. Therefore, the urgent development of specific antiviral drugs against this virus is imperative.


The nucleocapsid protein (NP) of SARS-CoV-2 is a highly basic RNA-binding protein that plays an essential role in viral replication, packaging of viral genomic RNA (gRNA), and modulation of the host cell response to infection². The SARS-CoV-2 NP comprises an N-terminal domain (NTD), a C-terminal domain (CTD), and three intrinsically disordered regions (IDRs): IDR_{NTD}, IDR_{central}, and IDR_{CTD}^{3,4} (Figure 1A). Sequence alignment has revealed that the NP sequence is highly conserved across various variants of SARS-CoV-2, including Alpha, Beta, Gamma, Delta, Lambda, and Omicron (Figure 1B). Targeting such a conserved protein could help mitigate viral

resistance, making the SARS-CoV-2 NP an ideal target for antiviral drug discovery.

Liquid-liquid phase separation (LLPS) of biomacromolecules refers to the phenomenon where proteins and nucleic acids condense into aggregates through multivalent interactions, forming semi-liquid and semi-solid compartments that are distinct from the surrounding liquid^{5,6}. Viruses exploit LLPS during their replication cycle to create membraneless organelles from nucleic acids and proteins, isolating them from other cellular components⁷⁻⁹. Since 2020, research has shown that the SARS-CoV-2 NP can condense with RNA and undergo LLPS to form protein-RNA aggregates¹⁰⁻¹⁶. Subsequent studies suggest that LLPS mediated by SARS-CoV-2 NP is a crucial mechanism for its involvement in virus assembly, replication, and immune regulation¹⁷⁻²¹. Targeting the SARS-CoV-2 NP and its associated LLPS could emerge as a promising strategy for developing antiviral therapies for COVID-19.

Current research has identified multiple classes of bioactive molecules targeting the SARS-CoV-2 nucleocapsid protein (NP) (structures in Figure 1C), which can be categorised into three mechanistic groups. First, molecules directly modulating NP liquid-liquid phase separation (LLPS) include: (-)-gallic acid gallate (GCG), which disrupts NP LLPS and inhibits viral replication *in vitro* (IC₅₀ = 44.4 μM)²²; ATP, a competitive regulator of NP-nucleic acid LLPS (IC₅₀ > 1 mM)²³; CVL218 and PJ34, enhancers of NP LLPS with CVL218 synergizing

CONTACT Yimin Li  2051058@sntcm.edu.cn  College of Pharmacy and Key Laboratory for Research and Development of "Qin Medicine" of Shaanxi Administration of Chinese Medicine, Shaanxi University of Chinese Medicine, Xixian New District, China; Xiaojun Xu  xuxiaojun@jsut.edu.cn  Institute of Bioinformatics and Medical Engineering, School of Electrical and Information Engineering, Jiangsu University of Technology, Changzhou 213001, China

 Supplemental data for this article can be accessed online at <https://doi.org/10.1080/14756366.2025.2501743>.

© 2025 Jiangsu University of Technology. Published by Informa UK Limited, trading as Taylor & Francis Group.

This is an Open Access article distributed under the terms of the Creative Commons Attribution-NonCommercial License (<http://creativecommons.org/licenses/by-nc/4.0/>), which permits unrestricted non-commercial use, distribution, and reproduction in any medium, provided the original work is properly cited. The terms on which this article has been published allow the posting of the Accepted Manuscript in a repository by the author(s) or with their consent.

A



B

	1	10	20	30	40	50	60	70	80
reference_WIV04	MS	LDNGPQNRNAP	RITFFGGPSDSTGNSNQC	ERS	GARSKQRRPOGLPNNNTASWFTALTQHGKE	DLKFP	RGQGV	INTNS	SDDOI
Alfa_B.1.1.7	MS	LDNGPQNRNAP	RITFFGGPSDSTGNSNQC	ERS	GARSKQRRPOGLPNNNTASWFTALTQHGKE	DLKFP	RGQGV	INTNS	SDDOI
Beta_B.1.351	MS	LDNGPQNRNAP	RITFFGGPSDSTGNSNQC	ERS	GARSKQRRPOGLPNNNTASWFTALTQHGKE	DLKFP	RGQGV	INTNS	SDDOI
Gamma_P.1	MS	LDNGPQNRNAP	RITFFGGPSDSTGNSNQC	ERS	GARSKQRRPOGLPNNNTASWFTALTQHGKE	DLKFP	RGQGV	INTNS	SDDOI
Delta_B.1.617.2	MS	LDNGPQNRNAP	RITFFGGPSDSTGNSNQC	ERS	GARSKQRRPOGLPNNNTASWFTALTQHGKE	DLKFP	RGQGV	INTNS	SDDOI
lamda_C.37	MS	LDNGPQNRNAP	RITFFGGPSDSTGNSNQC	ERS	GARSKQRRPOGLPNNNTASWFTALTQHGKE	DLKFP	RGQGV	INTNS	SDDOI
Omicron_B.1.1.529	MS	LDNGPQNRNAP	RITFFGGPSDSTGNSNQC	ERS	GARSKQRRPOGLPNNNTASWFTALTQHGKE	DLKFP	RGQGV	INTNS	SDDOI
Omicron_XBB.1.5	MS	LDNGPQNRNAP	RITFFGGPSDSTGNSNQC	ERS	GARSKQRRPOGLPNNNTASWFTALTQHGKE	DLKFP	RGQGV	INTNS	SDDOI

	90	100	110	120	130	140	150	160
reference_WIV04	GYRRATRRIRGGDGKMKDLS	SPRWYFYLLGTGPEAGLPYGANKDGI	IWVATEGALNTPKDHIGTRNPANNA	IVLQLPQGTTL				
Alfa_B.1.1.7	GYRRATRRIRGGDGKMKDLS	SPRWYFYLLGTGPEAGLPYGANKDGI	IWVATEGALNTPKDHIGTRNPANNA	IVLQLPQGTTL				
Beta_B.1.351	GYRRATRRIRGGDGKMKDLS	SPRWYFYLLGTGPEAGLPYGANKDGI	IWVATEGALNTPKDHIGTRNPANNA	IVLQLPQGTTL				
Gamma_P.1	GYRRATRRIRGGDGKMKDLS	SPRWYFYLLGTGPEAGLPYGANKDGI	IWVATEGALNTPKDHIGTRNPANNA	IVLQLPQGTTL				
Delta_B.1.617.2	GYRRATRRIRGGDGKMKDLS	SPRWYFYLLGTGPEAGLPYGANKDGI	IWVATEGALNTPKDHIGTRNPANNA	IVLQLPQGTTL				
lamda_C.37	GYRRATRRIRGGDGKMKDLS	SPRWYFYLLGTGPEAGLPYGANKDGI	IWVATEGALNTPKDHIGTRNPANNA	IVLQLPQGTTL				
Omicron_B.1.1.529	GYRRATRRIRGGDGKMKDLS	SPRWYFYLLGTGPEAGLPYGANKDGI	IWVATEGALNTPKDHIGTRNPANNA	IVLQLPQGTTL				
Omicron_XBB.1.5	GYRRATRRIRGGDGKMKDLS	SPRWYFYLLGTGPEAGLPYGANKDGI	IWVATEGALNTPKDHIGTRNPANNA	IVLQLPQGTTL				

	170	180	190	200	210	220	230	240	250
reference_WIV04	KGFYAE	GSRGGSQASSRSSRSRNSRNSTP	GSS	RGT	SPARMAGNGGDAALALLLLDRLN	QLESKM	SGKG	QQQGGQ	TVT
Alfa_B.1.1.7	KGFYAE	GSRGGSQASSRSSRSRNSRNSTP	GSS	RGT	SPARMAGNGGDAALALLLLDRLN	QLESKM	SGKG	QQQGGQ	TVT
Beta_B.1.351	KGFYAE	GSRGGSQASSRSSRSRNSRNSTP	GSS	RGT	SPARMAGNGGDAALALLLLDRLN	QLESKM	SGKG	QQQGGQ	TVT
Gamma_P.1	KGFYAE	GSRGGSQASSRSSRSRNSRNSTP	GSS	RGT	SPARMAGNGGDAALALLLLDRLN	QLESKM	SGKG	QQQGGQ	TVT
Delta_B.1.617.2	KGFYAE	GSRGGSQASSRSSRSRNSRNSTP	GSS	RGT	SPARMAGNGGDAALALLLLDRLN	QLESKM	SGKG	QQQGGQ	TVT
lamda_C.37	KGFYAE	GSRGGSQASSRSSRSRNSRNSTP	GSS	RGT	SPARMAGNGGDAALALLLLDRLN	QLESKM	SGKG	QQQGGQ	TVT
Omicron_B.1.1.529	KGFYAE	GSRGGSQASSRSSRSRNSRNSTP	GSS	RGT	SPARMAGNGGDAALALLLLDRLN	QLESKM	SGKG	QQQGGQ	TVT
Omicron_XBB.1.5	KGFYAE	GSRGGSQASSRSSRSRNSRNSTP	GSS	RGT	SPARMAGNGGDAALALLLLDRLN	QLESKM	SGKG	QQQGGQ	TVT

	260	270	280	290	300	310	320	330
reference_WIV04	EASKKP	PROKRTATKAYNVTQAF	GRRGPEQTQGNFGDQELIR	QGTQDYKHWPQIAQFAPSASAFFGMSRIGMEVTPSGTWLTYTGA				
Alfa_B.1.1.7	EASKKP	PROKRTATKAYNVTQAF	GRRGPEQTQGNFGDQELIR	QGTQDYKHWPQIAQFAPSASAFFGMSRIGMEVTPSGTWLTYTGA				
Beta_B.1.351	EASKKP	PROKRTATKAYNVTQAF	GRRGPEQTQGNFGDQELIR	QGTQDYKHWPQIAQFAPSASAFFGMSRIGMEVTPSGTWLTYTGA				
Gamma_P.1	EASKKP	PROKRTATKAYNVTQAF	GRRGPEQTQGNFGDQELIR	QGTQDYKHWPQIAQFAPSASAFFGMSRIGMEVTPSGTWLTYTGA				
Delta_B.1.617.2	EASKKP	PROKRTATKAYNVTQAF	GRRGPEQTQGNFGDQELIR	QGTQDYKHWPQIAQFAPSASAFFGMSRIGMEVTPSGTWLTYTGA				
lamda_C.37	EASKKP	PROKRTATKAYNVTQAF	GRRGPEQTQGNFGDQELIR	QGTQDYKHWPQIAQFAPSASAFFGMSRIGMEVTPSGTWLTYTGA				
Omicron_B.1.1.529	EASKKP	PROKRTATKAYNVTQAF	GRRGPEQTQGNFGDQELIR	QGTQDYKHWPQIAQFAPSASAFFGMSRIGMEVTPSGTWLTYTGA				
Omicron_XBB.1.5	EASKKP	PROKRTATKAYNVTQAF	GRRGPEQTQGNFGDQELIR	QGTQDYKHWPQIAQFAPSASAFFGMSRIGMEVTPSGTWLTYTGA				

C

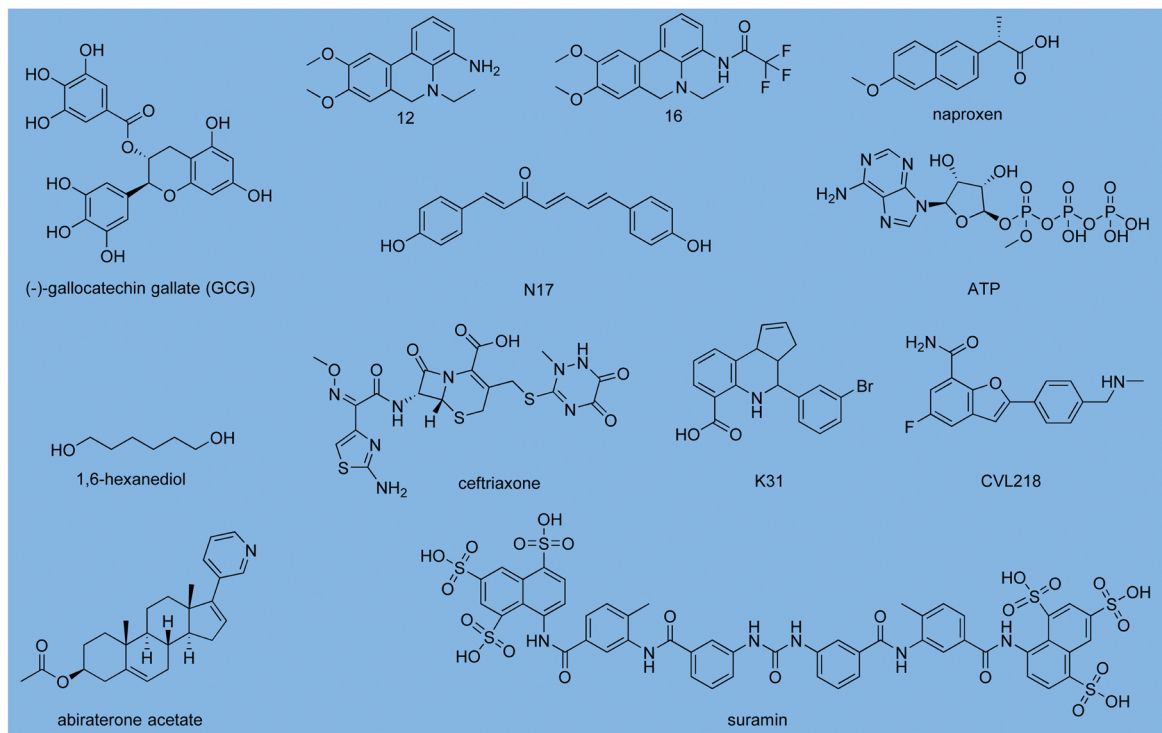


Figure 1. The sequence of the SARS-CoV-2 nucleocapsid protein (NP) is highly conserved across various variants of the novel coronavirus (A) Schematic representation of the domain structure of the SARS-CoV-2 NP. (B) Multiple sequence alignment of the N protein of coronaviruses. (C) Structures of representative small-molecule compounds targeting the SARS-CoV-2 NP.

remdesivir to amplify antiviral effects²⁴; the D-retroinverso isoform NIP-V targeting the NP CTD to disrupt LLPS¹⁹; 1,6-hexanediol suppressing both LLPS and NF- κ B signalling²⁵; and G12 RNA blocking

NP-RNA binding and preventing NP LLPS formation²⁶. Second, inhibitors of NP-RNA interactions comprise ceftriaxone, which blocks RNA binding to the NP NTD and RNP assembly²⁷; suramin,

disrupting NP NTD-RNA interaction ($K_d = 2.74\mu\text{M}$ via bio-layer interferometry assay)²⁸; and K31, a non-competitive inhibitor of NP-genomic RNA binding with antiviral activity (selective index ≈ 58)²⁹. Third, molecules directly targeting NP structural domains feature compounds 12/16 (binding Tyr109 in the NTD to inhibit replication)³⁰; N-17, a diphenylheptane with potent anti-SARS-CoV-2 activity ($\text{EC}_{50} = 0.17\mu\text{M}$)³¹; and abiraterone acetate, identified via *in silico* screening to attenuate viral replication through NP NTD interference³². These findings collectively validate the SARS-CoV-2 NP as a druggable target for antiviral development.

In this study, we present an assay based on homogeneous time-resolved fluorescence (HTRF) to identify small molecules that interact with the SARS-CoV-2 NP and modulate its LLPS. We identified two compounds as potential blockers of the NP-RNA interaction. Bio-layer interferometry (BLI) assays confirm that both compounds bind to the NP CTD rather than the NP NTD. Finally, fluorescence recovery after photobleaching (FRAP) experiments indicated that sennoside B disrupts the LLPS of the SARS-CoV-2 NP, suggesting that it may interfere with NP-mediated RNA packaging and contribute to the development of pharmacological strategies for combating SARS-CoV-2.

Materials and methods

Reagents

HTRF reagents, including anti-His₆-Eu cryptate (#61HISKLA) and streptavidin-conjugated XL665 (#610SAXLF) were purchased from CisBio (Bedford, MA). A range of compounds, including (-)-gallic acid (#HY-N0522), PJ34 (#HY-13688A), naproxen (#HY-15030), umifenovir (#HY-14904), ipratropium bromide (#HY-B0241), formoterol (#HY-B0010), disulphiram (#HY-B0240), iodoacetamide (#HY-34477), N-ethylmaleimide (#HY-D0843), tetramethylthiuram disulphide (TMTD), ABT-199 (#HY-15531), erlotinib (#HY-50896), ebselen (#HY-13750), ciclesonide, taurocholic acid (#HY-B1788), glycodeoxycholic acid (#HY-125731), cholic acid (#HY-N0324), sennoside A (#HY-N0365), sennoside B (#HY-N0366), and PF74 (#HY-120072) were obtained from MedChem Express (Shanghai, China). *Escherichia coli* BL21 (DE3) (#EE1002M) was obtained from Shanghai Weidi Biotechnology Co., Ltd. (Shanghai, China). Protease inhibitor cocktail (#A32965) was purchased from Thermo Fisher Scientific Inc. Streptavidin (SA) biosensors were sourced from Sartorius (Shanghai, China), and black 96-well microplates supplied by Greiner Bio-One (Darmstadt, Germany). White 384-shallow well microplates were acquired from PerkinElmer (Boston, MA, USA). HisCap 6FF prepacked columns were obtained from Smart Lifesciences (Changzhou, China), and a Superdex 200 Increase 10/300 GL column was purchased from Cytiva (Shanghai, China). A 5'-biotinylated RNA oligonucleotide (UCUAAACGAAC) was obtained from GENEWIZ (Suzhou, China).

Bioinformatics analysis

Multiple sequence alignment of the NP of coronaviruses was performed using CLUSTALW (<https://www.genome.jp/tools-bin/clustalw>) and the figure was generated with ESPript (<https://esprict.ibcp.fr/ESPript/ESPript/>).

Protein expression and purification

The full-length gene of SARS-CoV-2 NP (residues 1 to 419) was cloned into the pET-28a plasmid at the EcoR I and Xho I sites

(designated as pET28-NP FL) and kindly provided by the Guangdong Medical Laboratory Animal Centre (Guangzhou, China). Constructs for SARS-CoV-2 NP NTD (residues 44 to 174) and SARS-CoV-2 NP CTD (residues 247 to 364) were amplified by PCR from the plasmid pET28-NP FL and inserted into the NdeI-XhoI sites of the pET-28a vector to facilitate expression of proteins with a hexa-histidine (His₆) tag at the N-terminus. The plasmids were transformed into *Escherichia coli* BL21 (DE3) and grown in ampicillin-containing lysogeny broth (LB) media until reaching an OD_{600} of 0.8 at 37°C. Induction was performed using 0.5 mM IPTG, followed by further growth for 16 h at 18°C before harvesting by centrifugation. For purification, harvested cells were resuspended and sonicated in buffer A (25 mM HEPES, pH 7.5, 1 M NaCl, 5 mM MgCl₂, 10% glycerol, 5 mM β -mercaptoethanol, 5 mM imidazole, supplemented with a protease inhibitor cocktail at a 1:100 dilution). The lysate was clarified by centrifugation at 45,000g for 30 min at 4°C. The supernatant was loaded onto a HisCap 6FF metal affinity chromatography column, washed with buffer B (25 mM HEPES, pH 7.5, 300 mM NaCl, 5 mM MgCl₂, 10% glycerol, 5 mM β -mercaptoethanol, 20 mM imidazole), and eluted in buffer C (25 mM HEPES, pH 7.5, 300 mM NaCl, 5 mM MgCl₂, 10% glycerol, 5 mM β -mercaptoethanol, 300 mM imidazole). Proteins were concentrated using centrifugal concentrators and further purified by size-exclusion chromatography (Superdex 200 Increase 10/300 GL column) in gel filtration buffer (25 mM HEPES, pH 7.5, 300 mM NaCl, 5 mM MgCl₂, 10% glycerol, 1 mM DTT). Purified proteins were quantified using spectrophotometry (A260/A280 ratios below 0.55) and stored in aliquots that were flash-frozen in liquid nitrogen at -80°C.

In vitro SARS-CoV-2 N-RNA interaction assay

A homogeneous time-resolved fluorescence resonance energy transfer (HTRF) assay was utilised to measure the NP-RNA interaction. The experiment was conducted in white 384-shallow well microplates using phosphate-buffered saline (PBS) supplemented with 0.05% Tween 20. The assay involved the addition of 1 μL reaction buffer, 2 μL biotin-RNA (biotin-UCUAAACGAAC), and 2 μL His₆-tagged SARS-CoV-2 N protein (His-N) to each well. After a 1-h incubation at room temperature, 5 μL mixture of anti-His₆-Eu cryptate (as fluorescent donor) and XL665-conjugated streptavidin (as fluorescent acceptor) in assay buffer with 100 mM potassium fluoride was added. After incubation at room temperature (RT) for 1 h, the plate was read using an Envision multilabel reader. Raw counts (in counts *per s*, cps) at 665 nm and 620 nm were collected, and the signal value was expressed as the ratio of (cps at 665 nm/cps at 620 nm) \times 1000. DMSO was used as a negative control, while buffer served as a positive control. Prior to adding the assay mixture, compounds were dispensed into each well of the 384-well plate. GraphPad Prism software was used to visualise dose-response curves and calculate IC_{50} values. The Z' -factor³³ was calculated to assess assay quality, with a value >0.5 indicating a robust assay.

Bio-layer interferometry (BLI) binding experiments

BLI studies were performed using an Octet RED96 system in black 96-well plates with a kinetic buffer (PBS containing 0.01% Tween-20). The total working volume for samples or buffer was 200 μL *per well*, and all binding studies were conducted at 30°C with continuous shaking at 1000 $\times g$. Prior to each assay, streptavidin (SA) biosensor tips were immersed in 200 μL of kinetic buffer for at least 20 min at room temperature. Data were analysed using

FortBio data analysis software, with association and dissociation curves globally fitted using a simple 1:1 Langmuir model to determine the affinity constant (K_D).

For RNA-binding kinetics of the recombinant SARS-CoV-2 NP, biotinylated RNA (200 nM) was immobilised onto SA biosensors for 300 s. After establishing an initial baseline in the kinetics buffer (120 s), the sensors with RNA were exposed to varying concentrations of NP for 600 s of association, followed by a 1200-s dissociation period in the kinetics buffer.

To assess the effect of compounds on the interaction between NP and RNA, biotinylated ssRNA (50 nM) was coated on SA biosensors for 300 s. After an initial baseline step (60 s) in the kinetics buffer, the sensors were exposed to NP (50 nM) in the presence of varying concentrations of compounds (0, 6.25, 25, and 100 μ M) for 120 s of association, followed by a 120 s dissociation period in the kinetics buffer. Interference patterns from the biotinylated RNA with the buffer and uncoated biosensors containing a mixture of compounds and NP were analysed as two control sets. Double-reference subtracted data were utilised to calculate the binding constants.

Binding affinities of compounds to the SARS-CoV-2 NP, NP NTD, and NP CTD were also assessed using BLI. Each protein (0.39 mg/ml) was biotinylated in kinetic buffer at RT for 30 min. Biotinylated proteins were loaded onto SA biosensors by dipping the sensors into PCR tubes containing 15 μ l of biotin-protein (100 μ g/ml) for 20 min at room temperature. Following a baseline step (60 s), the sensors were immersed in increasing concentrations of compounds for 120 s of association, followed by a 300-s dissociation period in the kinetic buffer. Double-reference subtracted data were again used to calculate the binding constants with the Octet data analysis software.

In vitro phase separation assays

For the *in vitro* phase separation assays, the purified NP-mcherry was premixed with 1 \times reaction buffer (PBS with 2.5% PEG8000), then incubated with poly(I:C) or polyU for 15 min at 37°C. Each sample (10 μ l) was added into a Glass Bottom culture dish and imaged using a confocal microscope (TCSSP8STED3X, Leica). To obtain a higher solution photos, highlighted area was selected and 5 \times confocal zoom-in method was used to re-photograph the images.

Results

RNA-binding activity of SARS-CoV-2 NP

The SARS-CoV-2 NP is identified as an RNA-binding protein. Initially, a label-free biolayer interferometry (BLI) assay was employed to confirm its interaction with RNA. Recombinant SARS-CoV-2 NP was purified from *E. coli* with a purity exceeding 95%, as verified by 4–20% SDS-PAGE (Figure 2A). An 11-mer RNA sequence derived from the 5' transcriptional regulatory sequences (TRS) (UCUAAACGAAC) (Figure 2B), labelled with biotin, was utilised for the BLI assay, replacing viral RNA molecules. Biotinylated RNA was immobilised onto SA biosensor tips, and NP solutions were prepared at five different concentrations. The binding affinity yielded a dissociation constant (K_D) of 3.83 ± 0.04 nM, with a rate constant (k_{on}) of $2.19 \pm 0.07 \times 10^4$ (M \cdot s) $^{-1}$ and a dissociation rate constant (k_{off}) of $8.40 \pm 0.09 \times 10^{-5}$ s $^{-1}$ (Figure 2C,D). These findings indicate a direct physical interaction between the recombinant NP and the 11-mer TRS-derived RNA.

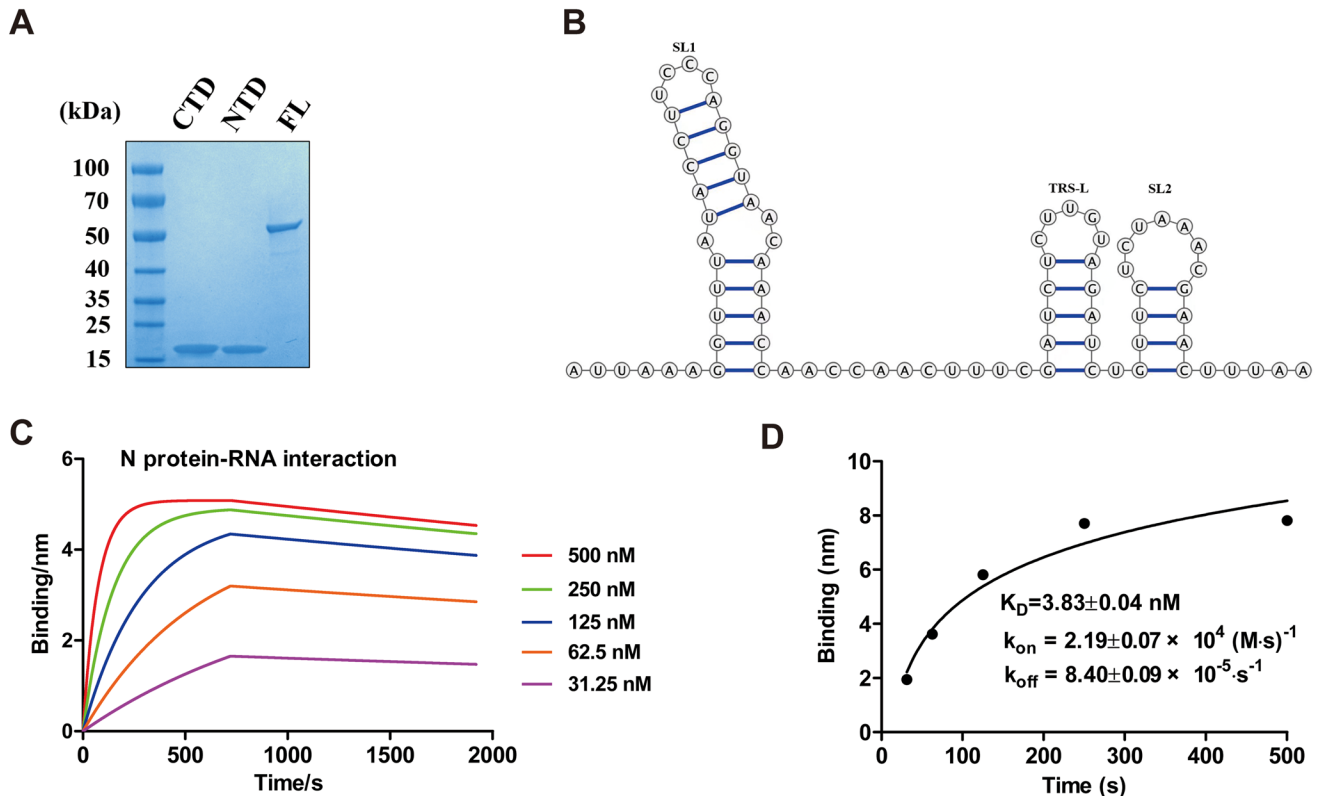


Figure 2. Recombinant SARS-CoV-2 NP binds to RNA *in vitro*. (A) SDS-PAGE analysis of purified full-length and truncated forms of NP. (B) Secondary structure of the 5' leader region sequences of the viral genome. (C) Representative binding kinetics of recombinant NP to RNA as determined by biolayer interferometry (BLI). The data are representative of three independent experiments. (D) The binding curve generated by fitting steady-state response levels at the end of the association phase versus NP concentration, with a dissociation constant (K_D) of 3.8 nM. Kinetic values calculated from $n=3$ experiments.

Development of an HTRF assay for SARS-CoV-2 NP-RNA interaction

Following confirmation of the SARS-CoV-2 NP-RNA interaction, we evaluated this interaction using an HTRF assay with Eu-anti His₆ antibody as the donor and XL665-conjugated streptavidin as the acceptor. Upon excitation of the donor fluorophore at 340 nm, emitted energy is transferred to the acceptor fluorophore when in proximity, resulting in decreased emission at 620 nm and increased emission at 665 nm (Figure 3A). Cross-titration experiments were conducted to determine the optimal concentrations of NP and RNA, with the concentrations of the Eu-anti His₆ antibody and XL665-conjugated streptavidin fixed at a 500-fold dilution. Key parameters for the assay include maximising the signal-to-background (S/B) ratio and maintaining protein concentrations within the linear range of the curve to avoid the hook effect. As shown in Figure 3B, the hook effect became evident at concentrations of 50 nM His₆-NP and higher, where excess His₆-NP competed for binding to RNA, inhibiting the signal. With the His₆-N concentration fixed at 50 nM, S/B ratios were calculated at varying RNA concentrations (Figure 3C). Based on these results, we selected 50 nM His₆-N and 50 nM RNA for optimal S/B and

minimal peptide consumption. Under optimised conditions, the method yielded a Z' factor of 0.89 ± 0.05 , indicating the reliability of the HTRF-based assay for identifying drugs targeting the NP-RNA interaction.

To preliminarily assess the protocol efficacy for drug screening applications, we tested two compounds GCG and PJ34 (chemical structures shown in Figure 3D,E), which were previously reported to interfere with the NP-RNA binding^{21,29}. Results indicated that GCG, at 50 μ M, nearly completely inhibited the NP-RNA interaction, whereas PJ34 had negligible effects (Figure 3F). Dose-response studies revealed that GCG's inhibition of the NP-RNA interaction was dose-dependent, with a half-maximal inhibitory concentration (IC₅₀) of $0.68 \pm 0.09 \mu$ M (Figure 3G). Subsequently, we assessed the competitive inhibition of the NP-RNA interaction by GCG and PJ34 using a BLI assay. GCG inhibited RNA binding to immobilised NP at 6.25 μ M, reducing the BLI signal (Figure 3H), while PJ34 only showed a decrease in signal at 100 μ M, corroborating previous results (Figure 3I). Serial dilution of GCG established its affinity constant (K_D) with NP at 3880 ± 290 nM (Figure 3J), confirming GCG as an effective inhibitor of the NP-RNA interaction and validating the efficacy of the established screening method.

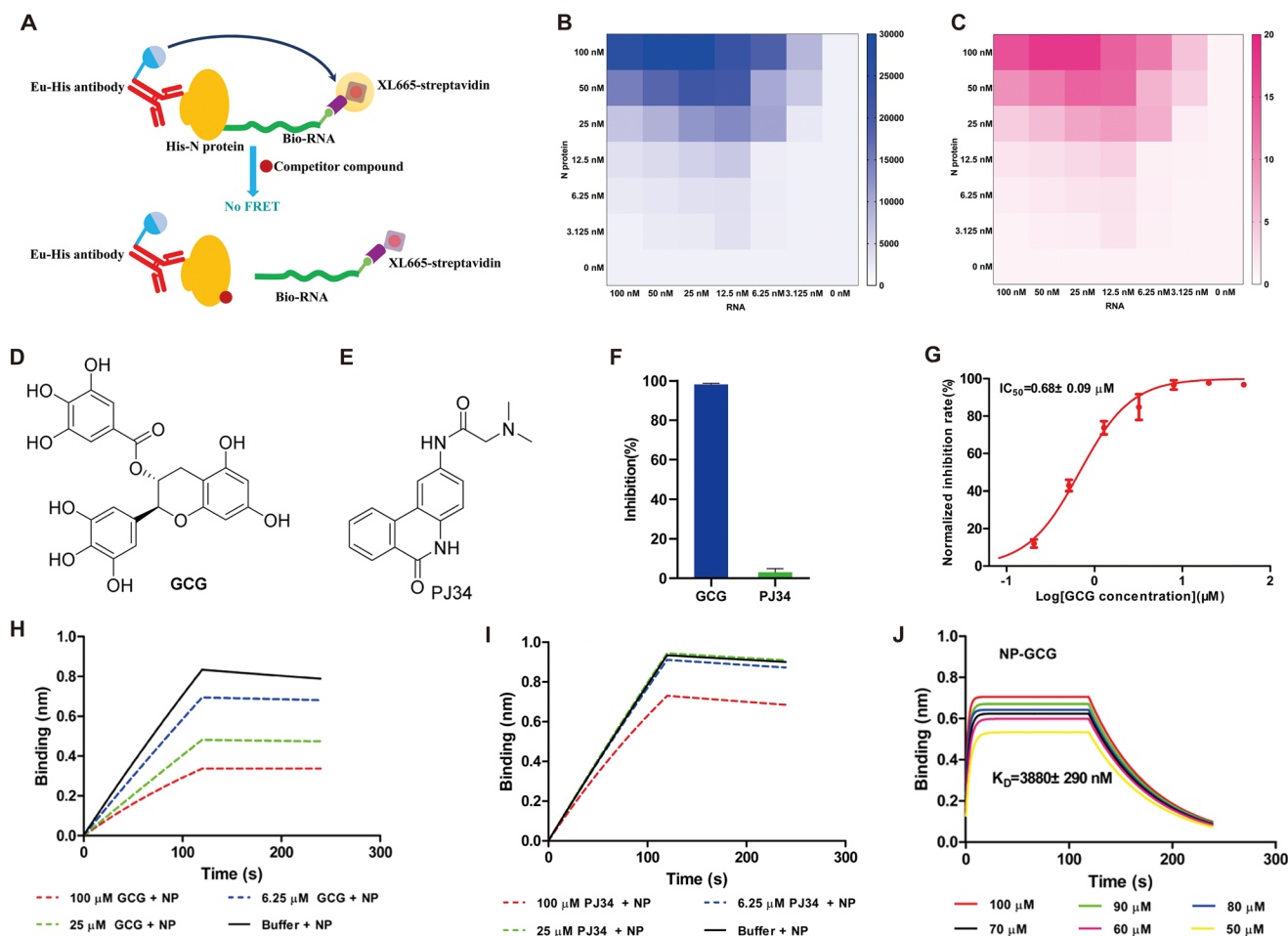


Figure 3. Development of a HTRF-based assay for screening inhibitors of the SARS-CoV-2 NP-RNA interaction. (A) Schematic representation of the HTRF assay principle. (B) Cross-titration of His₆-NP binding to biotin-labelled RNA, showing HTRF signal intensity from low (white) to high (blue). (C) Signal-to-background (S/B) ratio comparison generated from NP-RNA cross-titration. (D) and (E) Chemical structure of GCG and PJ34. (F) Comparison of the inhibitory effects of GCG and PJ34 at 50 μ M on NP-RNA interaction. (G) Dose-response curves of GCG for inhibition of NP-RNA interaction, presented as mean \pm SD from three independent experiments. (H) PJ34 disrupts the NP-RNA interaction at a higher concentration (100 μ M). (I) GCG disrupts the NP-RNA interaction at a lower concentration (6.25 μ M). (H) and (I) biosensors immobilised with RNA were incubated with NP in the presence of control DMSO or compound, and binding to the biosensor was monitored for 120 s via wavelength shift. (J) Binding affinity determined using a BLI assay between GCG and SARS-CoV-2 NP.

Sennoside A and sennoside B disrupt RNA binding to SARS-CoV-2 NP

Utilising the developed HTRF assay, we evaluated 18 compounds for their activity against the NP-RNA interaction. Compound information, including names, chemical types, purity, structures and sources, are presented in Table S1. At 50 μM , sennoside A and sennoside B demonstrated inhibition rates exceeding 98%, while the other 16 compounds displayed inhibition rates below 40% (Figure 4A). The structures of sennoside A and sennoside B are illustrated in Figure 4B,C. Dose-response studies showed that both compounds inhibited the NP-RNA interaction in a dose-dependent manner, with IC_{50} values of $3.17 \pm 0.39 \mu\text{M}$ (Figure 4D) and $1.05 \pm 0.23 \mu\text{M}$ (Figure 4H), respectively.

Sennoside A and sennoside B binds directly to SARS-CoV-2 NTD

Given the substantial inhibition of the NP-RNA interaction by sennoside A and sennoside B, we employed BLI technology to ascertain their binding affinities to the NP. Results indicated strong binding of both compounds to NP, with affinity constants of $962 \pm 19 \text{ nM}$ (Figure 4E) and $765 \pm 12 \text{ nM}$ (Figure 4I), respectively. To determine which domain they bind to, we expressed the NTD and CTD domains of the NP *in vitro* and measured their binding affinities using BLI. Results indicated that neither sennoside A nor

sennoside B bound to the NP NTD (Figure 4G,K), but both exhibited strong affinity for the NP CTD, with affinity constants of $1820 \pm 30 \text{ nM}$ (Figure 4F) and $529 \pm 16 \text{ nM}$ (Figure 4J), respectively. Thus, sennoside A and sennoside B bound directly to the NP at the CTD.

Sennoside B inhibits LLPS of SARS-CoV-2 N protein

The NP undergoes liquid-liquid phase separation (LLPS) when induced by RNA. Since sennoside A and sennoside B inhibit the NP-RNA interaction, we hypothesised that they might also prevent RNA-induced LLPS of the NP *in vitro*. To test this, we expressed NP fused with mCherry and assessed the effects of sennoside A and sennoside B on NP LLPS using fluorescence recovery after photobleaching (FRAP) experiments. Results (Figure 5A,B) demonstrated that, compared to the DMSO control, sennoside B significantly inhibited RNA-induced LLPS of the NP, while sennoside A exhibited relatively weaker activity.

Discussion

The SARS-CoV-2 NP is not only a structural component of the virus but also plays a pivotal role in viral replication by interacting with vRNA¹². To identify inhibitors of this interaction, we developed a screening system utilising the HTRF. Through a combination of

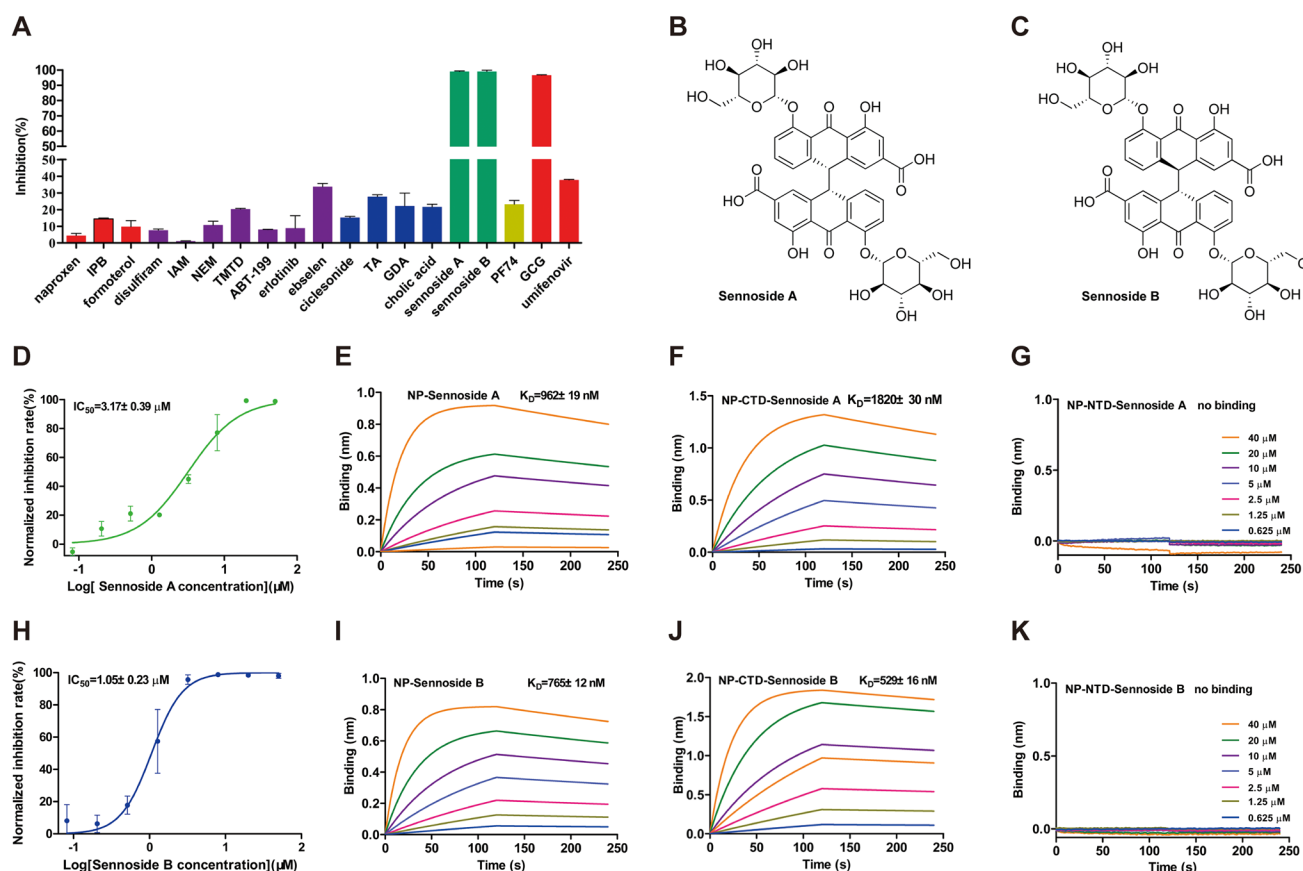


Figure 4. Sennoside A and Sennoside B inhibit the SARS-CoV-2 NP-RNA interaction. (A) Comparison of the inhibitory effects of various compounds on the NP-RNA interaction, presented as averages \pm standard deviation for $n=3$ independent experiments. (B) and (C) Chemical structure of Sennoside A and Sennoside B. (D) and (H) Dose-response curves of Sennoside A and Sennoside B for the inhibition of NP-RNA interaction. (E), (F) and (G) Representative binding sensorgrams depicting the interaction of Sennoside A with full-length NP, CTD and NTD as assessed by BLI. (I), (J), and (K) Representative binding sensorgrams depicting the interaction of Sennoside B with full-length NP, CTD and NTD as assessed by BLI. The results were determined from three independent experiments.

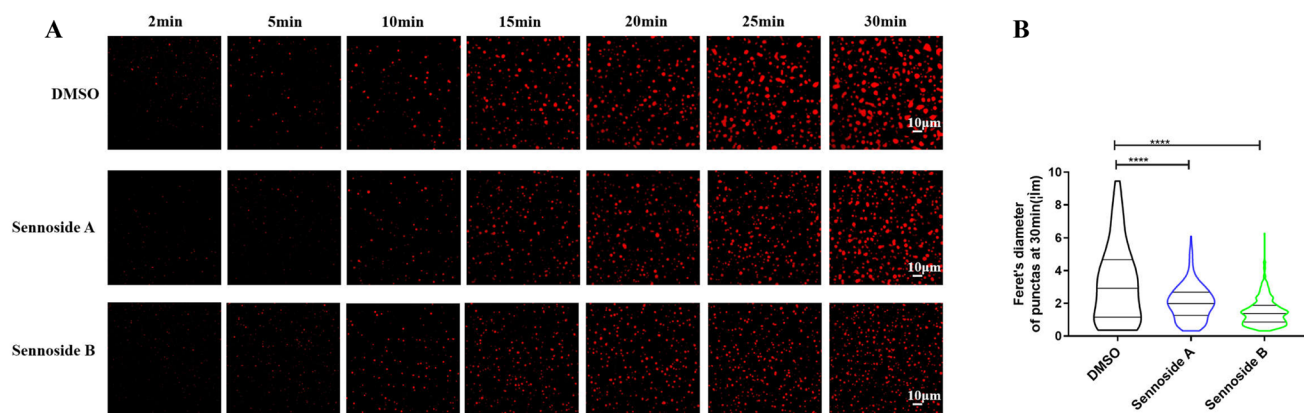


Figure 5. Sennoside B inhibits the liquid-liquid phase separation (LLPS) of NP. (A) Confocal microscopy images of NP droplets in the absence and presence of Sennoside A or Sennoside B, with DMSO (1%, v/v) used as the vehicle control. (B) Quantification of NP droplet diameter in the absence and presence of Sennoside A, Sennoside B, or DMSO, with a minimum of 150 droplets counted for each treatment group (*** $p < 0.001$).

Table 1. Affinity constant determination of SARS-CoV-2 nucleocapsid protein binding to RNA in representative research.

Method	K_D (nM)	Sequence (5'→3')	Type	Modification	Reference
FP	124.2 ± 6.5	CACUCACUGUCUUUUUGAUGGUAGAGU	Stem loop	FITC	34
	498.4 ± 43.2	CACUCACUGUCAAAAAGAUGGUAGAGU	Stem loop	FITC	
	148.6 ± 7.1	CACUCACUGUCUUUUUU	ssRNA	FITC	
	9728 ± 2353	CACUCACUGUC	ssRNA	FITC	
MST	5100 ± 600	UCUAAACGAAC	ssRNA	free	35
EMSA	560 ± 60	CACUGAC	ssRNA	FAM	36
	480 ± 30	CACUGAC/GUCAGUG	dsRNA	FAM	
FP	7 ± 1	UUUACCCUCCUUUCAGUUU	ssRNA	FITC	25
	51 ± 4	GGAAGAUUAAUUAUUUCC	ssRNA		
BLI	3.83 ± 0.04	UCUAAACGAAC	ssRNA	biotin	This paper

biochemical and biophysical approaches, we discovered that the natural product sennoside B effectively inhibits the NP-RNA interaction and also impedes RNA-induced liquid-liquid phase separation (LLPS) of the NP.

We first recombinantly expressed and purified the full-length SARS-CoV-2NP *in vitro* and verified its RNA-binding activity using biolayer interferometry (BLI). The results demonstrated that the NP exhibits strong RNA-binding activity. Over the past few years, numerous studies have employed various methods to assess the interaction between NP and RNA. Here, we focus exclusively on the measurement of the interaction between full-length NP and RNA, excluding truncated variants of the NP. As summarised in Table 1, these studies utilised different techniques, including fluorescence polarisation (FP), microscale thermophoresis (MST), electrophoretic mobility shift assay (EMSA), and BLI^{25,34–36}. Additionally, a diverse range of RNA types was tested, including stem-loop structured RNA, single-stranded RNA, double-stranded RNA. Due to differences in experimental methods and RNA structures, the reported binding affinity constants of N protein for RNA range from approximately 3 nM to 9000 nM. Even when the same method was used, studies by Mercaldi, Wu, and Zeng et al. reported different affinity values. In our study, we determined an affinity constant of approximately 3.8 nM, which closely aligns with the value (~7 nM) reported by Wu et al. using the FP method. Despite variations in the reported affinity values, all studies consistently support that recombinantly expressed NP exhibits RNA-binding activity, making it a valuable tool for further scientific research.

We screened 18 compounds for their activity against the NP-RNA interaction using our HTRF-based assay. Six of these compounds were derived from published studies, including GCG, PJ34, naproxen, umifenovir, ipratropium bromide, and formoterol. GCG, a

polyphenolic compound found in tea, was previously shown by Zhao et al.²² to inhibit both the binding of the NP to RNA and its LLPS, while also suppressing SARS-CoV-2 replication in A549-hACE2-Flag cells. In this study, GCG demonstrated significant inhibitory activity against the NP-RNA interaction. Similarly, Lin et al.³⁷ identified PJ34 through structure-based drug screening, which inhibited the binding of the NP of human coronavirus strain OC43 to RNA and suppressed viral replication. Peng et al.³⁸ noted that PJ34's binding site on the HCoV-OC43NP closely resembles its binding site on the SARS-CoV-2NP. However, in our experiments, PJ34 did not affect the SARS-CoV-2NP-RNA interaction, even at concentration as high as 50 µM. In contrast, Lin et al. reported that PJ34 inhibited the interaction between the HCoV-OC43 N protein and RNA at 10 µM³⁷. The differing electrostatic surface potentials between the HCoV-OC43 and SARS-CoV-2 N proteins may explain PJ34's higher binding affinity to the former, allowing it to inhibit NP-RNA interactions at lower concentrations³⁸. Naproxen, a nonsteroidal anti-inflammatory drug, was found by Terrier et al.³⁹ to bind to the NP's NTD and competitively inhibit RNA binding. While it demonstrated weak inhibitory effects on SARS-CoV-2 replication in Vero cells, it did not inhibit RNA-NP binding in our study. Similarly, umifenovir (Arbidol), identified by Hu et al.⁴⁰ as binding to the NP NTD, showed no inhibitory effect on NP-RNA interaction. Sarma et al. predicted that ipratropium bromide and formoterol could bind to the RNA-binding site of the N protein, but neither compound affected N-RNA interactions in our experiments⁴¹.

The SARS-CoV-2NP contains two structured domains, the NTD and C-terminal domain (CTD), both of which can bind RNA, in addition to three flanking intrinsically disordered regions (IDRs) that enhance RNA binding⁴. Regulation of NP LLPS is not confined to any specific domain, for instance, Lu et al.¹⁷ posited that the

IDR_{central} is critical for LLPS of NP, while Wang et al.¹⁶ and Luo et al.¹⁸ emphasised the indispensable role of IDR_{NTD}. Furthermore, Zhao et al. suggested that the NTD, CTD, and IDRs are all important for NP-RNA binding and LLPS, although the specific effects of different IDRs on NP LLPS remain undetermined²². Other studies also indicated that the CTD is crucial for NP LLPS. Our findings demonstrated that the small molecule sennoside B disrupted the LLPS of the NP by binding to its CTD, underscoring the critical role of this domain in NP function. This aligns with Wang et al., who designed a peptide derived from the CTD that effectively inhibited both LLPS and viral replication¹⁹. Although our findings indicate that sennoside B exhibits a strong inhibitory effect on N protein LLPS, we recognise our study has certain limitations. FRAP experiments alone are insufficient to comprehensively elucidate the molecular mechanisms underlying LLPS inhibition by sennoside B. Therefore, in future studies, we aim to perform more extensive cellular experiments to validate the effects of sennoside B on LLPS in a cellular context and to further investigate its potential impact on cellular functions and biological processes.

Sennosides A and B, anthraquinone glycosides extracted from rhubarb rhizomes and senna leaves, are isomers with identical molecular weights and formulas, differing only in the orientation of a shared substituent⁴². While primarily recognised for their laxative effects, mediated by the biotransformation of anthraquinones, previous studies indicated that sennoside A has a region-specific effect on spontaneous contractions in the colon⁴³, whereas sennoside B has been reported to inhibit platelet-derived growth factor receptor signalling and suppress PDGF-BB-induced proliferation of human osteosarcoma cells⁴⁴. During the preparation of this manuscript, we noted a study by Kumari et al. that reported sennoside A blocking the interaction between the NP and RNA, demonstrating its binding to the NP NTD⁴⁵. Our study corroborates that sennoside A inhibits the NP-RNA interaction, albeit through its interaction with the CTD. Additionally, we found that sennoside A disrupts NP LLPS, although its effect is weaker compared to sennoside B. Notably, Kumari et al.⁴⁵ did not assess whether sennoside A affects NP LLPS.

Conclusion

This study highlights the potential of sennoside B as an inhibitor that interacts with the CTD of SARS-CoV-2 NP, disrupting both its RNA-binding activity and LLPS. The isomer of sennoside B, sennoside A, can also inhibit the NP-RNA interaction, but its effect on RNA-induced N protein LLPS is weak. Sennoside B holds promise as a candidate for development as an anti-SARS-CoV-2 therapeutic by targeting NP. In the future, further research is needed to investigate the efficacy and safety of sennoside B in the treatment of COVID-19.

Authors contributions

Da-Wei Zhang: Validation, Investigation, Formal analysis Writing—original draft. Xiao-Shuang Xu, Liangxu Xie, Lei Xu: Investigation. Zhiguo Fu: Formal analysis. Yimin Li: Formal analysis, Writing—review and editing. Xiaojun Xu: Writing—original draft, Formal analysis, Writing—review and editing, Funding acquisition.

Laboratory health and safety statement

All mandatory laboratory health and safety procedures have been complied with in the course of conducting any experimental work

reported in this paper. In this study, we only carried experiments using the N protein of SARS-CoV-2 and did not involve any virus.

Disclosure statement

No potential conflict of interest was reported by the author(s).

Funding

The work is funded by National Natural Science Foundation of China [22003020], Changzhou Sci. & Tech. Program [CJ20200045], Xianyang young and middle-aged scientific and technological innovation leading talent project [L2022CXNLR009]; the Key Research and Development Program of Xianyang [L2023-ZDYF-SF-017].

ORCID

Xiaojun Xu  <http://orcid.org/0000-0002-6380-698X>

Data availability statement

The data presented in this study are available on request from the corresponding author.

References

1. Wu F, Zhao S, Yu B, Chen Y-M, Wang W, Song Z-G, Hu Y, Tao Z-W, Tian J-H, Pei Y-Y, et al. A new coronavirus associated with human respiratory disease in China. *Nature*. 2020;579(7798):265–269.
2. Cascarina SM, Ross ED. Phase separation by the SARS-CoV-2 nucleocapsid protein: consensus and open questions. *J Biol Chem*. 2022;298(3):101677.
3. Klein S, Cortese M, Winter SL, Wachsmuth-Melm M, Neufeldt CJ, Cerikan B, Stanifer ML, Boulant S, Bartenschlager R, Chlanda P. SARS-CoV-2 structure and replication characterized by in situ cryo-electron tomography. *Nat Commun*. 2020;11(1):5885.
4. Ye Q, West AM, Silletti S, Corbett KD. Architecture and self-assembly of the SARS-CoV-2 nucleocapsid protein. *Protein Sci*. 2020;29(9):1890–1901.
5. Boeynaems S, Alberti S, Fawzi NL, Mittag T, Polymenidou M, Rousseau F, Schymkowitz J, Shorter J, Wolozin B, Van Den Bosch L, et al. Protein phase separation: a new phase in cell biology. *Trends Cell Biol*. 2018;28(6):420–435.
6. Zhang H, Ji X, Li P, Liu C, Lou J, Wang Z, Wen W, Xiao Y, Zhang M, Zhu X. Liquid-liquid phase separation in biology: mechanisms, physiological functions and human diseases. *Sci China Life Sci*. 2020;63(7):953–985.
7. Etibor TA, Yamauchi Y, Amorim MJ. Liquid biomolecular condensates and viral lifecycles: review and perspectives. *Viruses*. 2021;13(3):366.
8. Gaete-Argel A, Márquez CL, Barriga GP, Soto-Rifo R, Valiente-Echeverría F. Strategies for success. Viral infections and membraneless organelles. *Front Cell Infect Microbiol*. 2019;9:336.
9. Nevers Q, Albertini AA, Lagaudrière-Gesbert C, Gaudin Y. Negri bodies and other virus membrane-less replication compartments. *Biochim Biophys Acta Mol Cell Res*. 2020;1867(12):118831.

10. Carlson CR, Asfaha JB, Ghent CM, Howard CJ, Hartooni N, Safari M, Frankel AD, Morgan DO. Phosphoregulation of phase separation by the SARS-CoV-2 N protein suggests a biophysical basis for its dual functions. *Mol Cell*. 2020;80(6):1092–1103.e4.
11. Chen H, Cui Y, Han X, Hu W, Sun M, Zhang Y, Wang PH, Song G, Chen W, Lou J. Liquid-liquid phase separation by SARS-CoV-2 nucleocapsid protein and RNA. *Cell Res*. 2020;30(12):1143–1145.
12. Cubuk J, Alston JJ, Incicco JJ, Singh S, Stuchell-Brereton MD, Ward MD, Zimmerman MI, Vithani N, Griffith D, Wagoner JA, et al. The SARS-CoV-2 nucleocapsid protein is dynamic, disordered, and phase separates with RNA. *Nat Commun*. 2021;12(1):1936.
13. Iserman C, Roden CA, Boerneke MA, Sealfon RSG, McLaughlin GA, Jungreis I, Fritch EJ, Hou YJ, Ekena J, Weidmann CA, et al. Genomic RNA elements drive phase separation of the SARS-CoV-2 nucleocapsid. *Mol Cell*. 2020;80(6):1078–1091.e6.
14. Perdikari TM, Murthy AC, Ryan VH, Watters S, Naik MT, Fawzi NL. SARS-CoV-2 nucleocapsid protein phase-separates with RNA and with human hnRNPs. *Embo J*. 2020;39(24):e106478.
15. Savastano A, Ibáñez de Opakua A, Rankovic M, Zweckstetter M. Nucleocapsid protein of SARS-CoV-2 phase separates into RNA-rich polymerase-containing condensates. *Nat Commun*. 2020;11(1):6041.
16. Wang J, Shi C, Xu Q, Yin H. SARS-CoV-2 nucleocapsid protein undergoes liquid-liquid phase separation into stress granules through its N-terminal intrinsically disordered region. *Cell Discov*. 2021;7(1):5.
17. Lu S, Ye Q, Singh D, Cao Y, Diedrich JK, Yates JR, III, Villa E, Cleveland DW, Corbett KD. The SARS-CoV-2 nucleocapsid phosphoprotein forms mutually exclusive condensates with RNA and the membrane-associated M protein. *Nat Commun*. 2021;12(1):502.
18. Luo L, Li Z, Zhao T, Ju X, Ma P, Jin B, Zhou Y, He S, Huang J, Xu X, et al. SARS-CoV-2 nucleocapsid protein phase separates with G3BPs to disassemble stress granules and facilitate viral production. *Sci Bull*. 2021;66(12):1194–1204.
19. Wang S, Dai T, Qin Z, Pan T, Chu F, Lou L, Zhang L, Yang B, Huang H, Lu H, et al. Targeting liquid-liquid phase separation of SARS-CoV-2 nucleocapsid protein promotes innate antiviral immunity by elevating MAVS activity. *Nat Cell Biol*. 2021;23(7):718–732.
20. Wu Y, Ma L, Cai S, Zhuang Z, Zhao Z, Jin S, Xie W, Zhou L, Zhang L, Zhao J, et al. RNA-induced liquid phase separation of SARS-CoV-2 nucleocapsid protein facilitates NF- κ B hyper-activation and inflammation. *Signal Transduct Target Ther*. 2021;6(1):167.
21. Zhao D, Xu W, Zhang X, Wang X, Ge Y, Yuan E, Xiong Y, Wu S, Li S, Wu N, et al. Understanding the phase separation characteristics of nucleocapsid protein provides a new therapeutic opportunity against SARS-CoV-2. *Protein Cell*. 2021;12(9):734–740.
22. Zhao M, Yu Y, Sun L-M, Xing J-Q, Li T, Zhu Y, Wang M, Yu Y, Xue W, Xia T, et al. GCG inhibits SARS-CoV-2 replication by disrupting the liquid phase condensation of its nucleocapsid protein. *Nat Commun*. 2021;12(1):2114.
23. Dang M, Li T, Song J. ATP and nucleic acids competitively modulate LLPS of the SARS-CoV2 nucleocapsid protein. *Commun Biol*. 2023;6(1):80.
24. Ge Y, Tian T, Huang S, Wan F, Li J, Li S, Wang X, Yang H, Hong L, Wu N, et al. An integrative drug repositioning framework discovered a potential therapeutic agent targeting COVID-19. *Signal Transduct Target Ther*. 2021;6:165.
25. Wu C, Qavi AJ, Hachim A, Kavian N, Cole AR, Moyle AB, Wagner ND, Sweeney-Gibbons J, Rohrs HW, Gross ML, et al. Characterization of SARS-CoV-2 nucleocapsid protein reveals multiple functional consequences of the C-terminal domain. *Iscience*. 2021;24(6):102681.
26. Sekine R, Tsuno S, Irokawa H, Sumitomo K, Han T, Sato Y, Nishizawa S, Takeda K, Kuge S. Inhibition of SARS-CoV-2 nucleocapsid protein-RNA interaction by guanosine oligomeric RNA. *J Biochem*. 2023;173(6):447–457.
27. Luan X, Li X, Li Y, Su G, Yin W, Jiang Y, Xu N, Wang F, Cheng W, Jin Y, et al. Antiviral drug design based on structural insights into the N-terminal domain and C-terminal domain of the SARS-CoV-2 nucleocapsid protein. *Sci Bull*. 2022;67(22):2327–2335.
28. Guo C, Xu H, Li X, Yu J, Lin D. Suramin disturbs the association of the N-terminal domain of SARS-CoV-2 nucleocapsid protein with RNA. *Molecules*. 2023;28(6):2534.
29. Royster A, Ren S, Ma Y, Pintado M, Kahng E, Rowan S, Mir S, Mir M. SARS-CoV-2 nucleocapsid protein is a potential therapeutic target for anticoronavirus drug discovery. *Microbiol Spectr*. 2023;11(3):e01186-23.
30. Wang Y-T, Long X-Y, Ding X, Fan S-R, Cai J-Y, Yang B-J, Zhang X-F, Luo R-H, Yang L, Ruan T, et al. Novel nucleocapsid protein-targeting phenanthridine inhibitors of SARS-CoV-2. *Eur J Med Chem*. 2022;227:113966.
31. Liu Y, Sa K, Xu W, Chen Y, Liang J, Zou P, Chen L. 1, 7-Bis (4-hydroxyphenyl)-1, 4, 6-heptatrien-3-one inhibits SARS-CoV-2 by targeting the nucleocapsid protein. *Acta Mater Med*. 2023;2:270–280.
32. Kim J, Hwang SY, Kim D, Kim M, Baek K, Kang M, An S, Gong J, Park S, Kandeel M, et al. Abiraterone Acetate Attenuates SARS-CoV-2 Replication by Interfering with the Structural Nucleocapsid Protein. *Biomol Ther*. 2022;30(5):427–434.
33. Zhang JH, Chung TD, Oldenburg KR. A simple statistical parameter for use in evaluation and validation of high throughput screening assays. *J Biomol Screen*. 1999;4(2):67–73.
34. Mercaldi GF, Bezerra EHS, Batista FAH, Tonoli CCC, Soprano AS, Shimizu JF, Nagai A, da Silva JC, Filho HVR, do Nascimento Faria J, et al. Discovery and structural characterization of chicoric acid as a SARS-CoV-2 nucleocapsid protein ligand and RNA binding disruptor. *Sci Rep*. 2022;12(1):18500.
35. Ni X, Han Y, Zhou R, Zhou Y, Lei J. Structural insights into ribonucleoprotein dissociation by nucleocapsid protein interacting with non-structural protein 3 in SARS-CoV-2. *Commun Biol*. 2023;6(1):193.
36. Ye Q, Lu S, Corbett KD. Structural basis for SARS-CoV-2 nucleocapsid protein recognition by single-domain antibodies. *Front Immunol*. 2021;12:719037.
37. Lin SY, Liu CL, Chang YM, Zhao J, Perlman S, Hou MH. Structural basis for the identification of the N-terminal domain of coronavirus nucleocapsid protein as an antiviral target. *J Med Chem*. 2014;57(6):2247–2257.
38. Peng Y, Du N, Lei Y, Dorje S, Qi J, Luo T, Gao GF, Song H. Structures of the SARS-CoV-2 nucleocapsid and their perspectives for drug design. *Embo J*. 2020;39(20):e105938.
39. Terrier O, Dilly S, Pizzorno A, Chalupska D, Humpolickova J, Bouřa E, Berenbaum F, Quideau S, Lina B, Fève B, et al. Antiviral properties of the NSAID drug naproxen targeting the nucleoprotein of SARS-CoV-2 coronavirus. *Molecules*. 2021;26(9):2593.
40. Hu X, Zhou Z, Li F, Xiao Y, Wang Z, Xu J, Dong F, Zheng H, Yu R. The study of antiviral drugs targeting SARS-CoV-2 nucleocapsid and spike proteins through large-scale compound repurposing. *Heliyon*. 2021;7(3):e06387.

41. Sarma P, Shekhar N, Prajapat M, Avti P, Kaur H, Kumar S, Singh S, Kumar H, Prakash A, Dhibar DP, et al. In-silico homology assisted identification of inhibitor of RNA binding against 2019-nCoV N-protein (N terminal domain). *J Biomol Struct Dyn*. 2021;39(8):2724–2732.
42. Hwang IY, Jeong CS. Gastroprotective activities of sennoside A and sennoside B via the up-regulation of prostaglandin E2 and the inhibition of H⁺/K⁺-ATPase. *Biomol Ther*. 2015;23(5):458–464.
43. Kobayashi M, Yamaguchi T, Odaka T, Nakamura T, Tsuchiya S, Yokosuka O, Yano S. Regionally differential effects of sennoside A on spontaneous contractions of colon in mice. *Basic Clin Pharmacol Toxicol*. 2007;101(2):121–126.
44. Chen YC, Chang CN, Hsu HC, Chiou SJ, Lee LT, Hseu TH. Sennoside B inhibits PDGF receptor signaling and cell proliferation induced by PDGF-BB in human osteosarcoma cells. *Life Sci*. 2009;84(25–26):915–922.
45. Kumari S, Mistry H, Bihani SC, Mukherjee SP, Gupta GD. Unveiling potential inhibitors targeting the nucleocapsid protein of SARS-CoV-2: structural insights into their binding sites. *Int J Biol Macromol*. 2024;273(Pt 2):133167.